NASA-CR-192224

SRI International

(NASA-CR-192224) STUDY OF AURORAL DYNAMICS WITH COMBINED SPACECRAFT AND INCOHERENT-SCATTER RADAR DATA Quarterly Progress Report No. 5, 1 Sep. - 31 Dec. 1992 (SRI International Corp.) 27 p

N93-26159

Unclas

G3/46 0160825

NAGW-3037
IN-46-CR
160825
P.27

Quarterly Progress Report 5 • 1 February 1993
Covering the Period 1 September through 31 December 1992

STUDY OF AURORAL DYNAMICS WITH COMBINED SPACECRAFT AND INCOHERENT-SCATTER RADAR DATA

Jürgen Watermann, Research Physicist
Geoscience and Engineering Center

SRI Project 2781

Prepared for:

Headquarters
National Aeronautics and Space Administration
Space Physics Division
Research and Analysis Support Program
Washington, D.C. 20546

Attn: Dr. D. Evans
Code SS

ORIGINAL CONTAINS
COLOR ILLUSTRATIONS

Contract NASW-4063

Approved:

James F. Vickrey, Director
Geoscience and Engineering Center

333 Ravenswood Avenue • Menlo Park, CA 94025-3493 • (415) 326-6200 • FAX: (415) 326-5512 • Telex: 334486

The Ionospheric Footprint Of Magnetosheath-Like Particle Precipitation Observed by an Incoherent-Scatter Radar

JÜRGEN WATERMANN
Geoscience and Engineering Center, SRI International, Menlo Park, California, U.S.A.

DIRK LUMMERZHEIM
Geophysical Institute, University of Alaska, Fairbanks, Alaska, U.S.A.

ODILE DE LA BEAUJARDIÈRE
Geoscience and Engineering Center, SRI International, Menlo Park, California, U.S.A.

PATRICK T. NEWELL
Applied Physics Laboratory, Johns Hopkins University, Laurel, Maryland, U.S.A.

FREDERIC J. RICH
Phillips Laboratory, Hanscom Air Force Base, Bedford, Massachusetts, U.S.A.

FOREWORD

This quarterly progress report consists of a draft of our recent study of coincident Sondrestrom incoherent-scatter radar and DMSP-F7 measurements made in the low-altitude cusp, which we briefly described in Monthly Technical Status Report 15 (16 December 1992). This paper will now be submitted to the *Journal of Geophysical* Research.

We have examined Sondrestrom incoherent-scatter radar observations of ionospheric plasma density and temperature distributions, as well as measurements of *F*-region ion drifts that were made during a prenoon pass by the DMSP-F7 satellite through the radar field of view. The spacecraft traversed a region of intense electron precipitation with a characteristic energy below approximately 200 eV. Particles with such low characteristic energies are believed to be directly or indirectly of magnetosheath origin. The precipitation region had a width of about 2° invariant latitude. The corotating radar observed a patch of enhanced electron density and elevated electron temperature in the *F2* region between about 10.5 and 12 magnetic local time in the same invariant latitude range where DMSP-F7 detected the soft-electron flux. The ion drift pattern, also obtained by radar, shows that it is unlikely that the plasma patch was produced by solar radiation and advected into the radar field of view. We suggest that the radar observed modifications of the ionospheric plasma distribution, which resulted from direct entry of magnetosheath electrons into the magnetosphere and down to ionospheric altitudes. Model calculations of the ionospheric response to the observed electron flux support our interpretation.

INTRODUCTION

Certain magnetopause boundary regions, including the cusps, the low-latitude boundary layer (LLBL) and the plasma mantle (PM), play an important role in the transfer of plasma and magnetic flux from the solar wind into the magnetosphere. The cusps are relatively small regions in the high-latitude noon sectors of both hemispheres. In closed magnetosphere models, these cusps connect the magnetopause neutral points with singular points in the ionosphere. In open magnetosphere models the magnetopause is interrupted in the exterior cusp, and the cusps form a funnel through which magnetosheath plasma has the most direct access to the ionosphere [cf. *Haerendel et al.*, 1978; *Kremser and Lundin*, 1990]. This terminology concurs with the conceptual cusp definition proposed by *Newell and Meng* [1988].

Owing to the large magnetopause surface and the relative scarcity of spacecraft observations in the magnetospheric boundary regions, *in-situ* observations of the boundary layers are not often available. To study boundary layer processes, it is helpful to use indirect measurements from low-altitude spacecraft and ground-based instruments. Low-altitude magnetospheric and ionospheric observations take advantage of the fact that the magnetospheric boundary layers map to a relatively small area in the high-latitude ionosphere (see, for instance, Figure 3 of *Lundin* [1991] for a graphic representation of statistical magnetospheric boundary layer footprints).

The conceptual definition of characterizing magnetospheric boundary regions by means of charged-particle properties is only one of several possibilities, although probably the most widely used. Other definitions are based on properties of various other physical observables. These include visible auroral emissions [*Sandholt et al.*, 1985; *Sivjee*, 1985; *McEwen*, 1985], coherent HF radar backscatter [*Baker et al.*, 1990], magnetic pulsations [*Engebretson et al.*, 1986; *Olson*, 1986], the correlation between optical emissions and geomagnetic pulsations [*McHarg and Olson*, 1992], VLF signal characteristics and ionospheric absorption of cosmic noise [*Engebretson et al.*, 1990], and field-aligned currents (consider, for instance, the current systems traditionally named 'cusp current' and 'mantle current,' e.g., *Bythrow et al.* [1988]).

Our paper deals with the identification of magnetospheric boundary regions from ground-based incoherent scatter radar observations. These boundary regions, which include the cusp, the LLBL, and the PM, are identified from the characteristics of particle precipitation observed on the DMSP-F7 spacecraft. We then analyze radar observations of the ionosphere made during several hours around the relevant satellite pass through the radar field of view to determine the properties of the ionospheric plasma within the region of magnetosheath-like electron precipitation. Using an auroral model to predict the ionospheric response to the observed electron precipitation, we find that the radar measurements indeed show plasma densities and temperatures that can be expected as a result of electron precipitation with a characteristic energy below some 200 eV.

To our knowledge, no work has been published except for the papers by *Kofman and Wickwar* [1984] and *Wickwar and Kofman* [1984] that addresses specifically the ionospheric signature of soft-electron precipitation near local noon, observed with an incoherent-scatter

radar. Both papers suggest particle precipitation as a possible source for the measured increases of thermal electron density and temperature in the ionospheric *F* region. However, no satellite observations of particle precipitation were available to confirm the suggestion.

OBSERVATIONS

We will focus our discussion on data taken on 28 June 1984 in the dayside ionosphere, during a 68-hour incoherent-scatter World Day experiment. The Sondrestrom incoherent-scatter radar [*Kelly*, 1983], which participated in this experiment, is located at 67° latitude and 309° longitude on the west coast of Greenland; the *E* region at 120-km altitude above the radar site is intersected by the 74°-invariant-latitude contour. During the experiment, the radar performed repetitive antenna cycles, which included an elevation scan followed by multiple fixed positions. In the elevation scans, the antenna moved with constant angular speed of 0.4°/s in a vertical plane perpendicular to the local L shell; a complete scan took 5 minutes. The elevation scans yield two-dimensional images of the plasma density and temperature distributions in the scan plane. During the multiposition part of the radar cycle, the antenna was kept fixed at each of eleven different positions for times varying between 30 s and 120 s, depending on the antenna elevation. In one of those positions, the radar beam was field-aligned; in three of the five pairs, the antenna was pointed poleward at 30°, 50°, and 65° elevation; in the remaining two pairs, it was directed equatorward at 50° and 30° elevation. A pair consists of two antenna positions (at a fixed elevation), one directed a few degrees to the west and the other a similar amount to the east of the magnetic meridian through Sondrestrom (which is found 27° counterclockwise from geographic north). The multiposition measurements yield estimates of the plasma convection pattern over a wide range of invariant latitudes, provided the plasma drift on a given *L* shell is uniform within the radar field of view.

The DMSP-F7 satellite moved poleward through the Sondrestrom radar field of view and, at 1124 UT, its *E*-region footprint crossed 74° invariant latitude some 130 km west of Sondrestrom. We will use electron- and ion-energy spectra measured aboard this satellite as our reference for determining the footprints of magnetospheric regions. The DMSP particle spectrometers [*Hardy et al.*, 1984] sample the electron and ion precipitation with 1-s resolution (equivalent to 7.4-km flight distance). Such a resolution is much better than the radar integration time of 20 s in this particular experiment, which is equivalent to 35-km integration distance at 280-km altitude. Because of this limitation, it is not possible to identify the boundaries of magnetospheric regions from radar observations with the same resolution as from spacecraft observations.

Figure 1 shows electron and ion spectrograms measured by DMSP-F7 between 1222 and 1226 UT. The figure contains four panels with a common UT and InvLat (Invariant Latitude) axes for the abscissa. All scales used along the ordinate are logarithmic. The upper panel shows the total energy flux *JE* of electrons (black) and ions (orange) in eV cm^{-2} s^{-1} sr^{-1}, the second panel shows the average energy *E* in eV of the electron and ion fluxes. The third panel shows the electron-energy spectrum in eV cm^{-2} s^{-1} sr^{-1} eV^{-1}, the intensity is color-coded. The bottom panel shows the ion-energy spectrum in the same units. (Note that the ordinate is inverted in the bottom panel and that the intensity ranges for electrons and ions extend over different orders of magnitude.) At top of the figure, we have indicated the magnetospheric regions as identified from particle characteristics, based on the criteria developed by *Newell and Meng* [1988, 1989].

DMSP-F7 first crossed a region of particles that were characteristic for the central plasma sheet (CPS); the spacecraft then encountered the low-altitude footprint of the LLBL, followed by the particle cusp and the PM. The precipitation poleward of the PM could not unambiguously be associated with a particular magnetospheric source region. Its spectral properties resemble those of PM precipitation; however, the precipitation is of unusually high intensity. Finally, the spacecraft entered the polar rain (PR) region. The cusp proper was detected around 1224 UT, near 10 MLT (magnetic local time), between 73.8° and 74.3° invariant latitude, and was traversed by the satellite within 8 s.

The identification of the magnetospheric cusp from particle measurements on low- and mid-altitude spacecraft relies on ion and electron flux properties [*Newell and Meng*, 1989; *Kremser and Lundin*, 1990]. Figure 1 shows that the intensity of the electron energy flux in the cusp and magnetospheric boundary layers (LLBL and PM) was between one and two orders of magnitude higher than the ion energy flux. Therefore, the ionospheric effects of cusp-like precipitation that we expect to find are caused mainly by the electron flux, and the contribution of the ion flux to variations in plasma density and temperature is deemed insignificant. In Figure 1, we notice a region of intense low-energy (30- to 500-eV) electron flux, which extends from the equatorward edge of the LLBL (at 73.2° invariant latitude) across the cusp and a part of the PM, up to 74.9° invariant latitude. The intensity of the electron flux is even lower in the cusp proper than in the adjacent LLBL and PM regions, and the average electron energy is slightly higher in the LLBL than in the cusp and PM. Because we expect the radar to be sensitive to the ionospheric signatures of the electron precipitation only, we treat this entire region of intense soft-electron precipitation as a single region and consider it characteristic of magnetosheath-like particle precipitation. In any case, the limited spatial resolution of the radar observations would hamper the exact identification of the boundaries between LLBL, cusp, and PM.

The geographic setting of the event is shown in Figure 2. The Sondrestrom radar location is marked by a full diamond labeled SSF. The line through the radar indicates the orientation of the elevation scan plane, the heavy section represents the scan trace at 120-km altitude, and its thin extension the scan trace at 350-km altitude. Dotted lines indicate *E* region (120-km altitude) contours of equal invariant latitudes. The DMSP-F7 trajectory mapped down to 120-km altitude is indicated by a thin line with diamond markers separating CPS, LLBL, cusp (heavily drawn), PM, the unidentified interval, and PR. The hatched segment spans the region of intense soft-electron precipitation, including LLBL, cusp, and the equatorward part of PM. No significant precipitation was measured beyond the equatorward and poleward end points of the satellite trajectory segment plotted here. The geometry of this event is such that the DMSP-F7 trajectory is approximately parallel to the radar elevation scan plane and perpendicular to the contours of constant invariant latitude.

A second heavily drawn segment close to the right margin of Figure 2 indicates cusp precipitation observed by DMSP-F7 on its preceding pass, 102 min earlier. The satellite identified the cusp at 10 MLT between 73.6° and 73.9° invariant, i.e., almost at the same invariant latitude as during its pass close to Sondrestrom. If we assume that the particle cusp did not move significantly in invariant latitude between these two passes, we expect its ionospheric footprint to be approximately overhead of the radar around the time of the nearby DMSP-F7

pass. In Figure 2, we have indicated by a hatched segment along the radar scan the interval where the radar detected enhanced electron density and elevated electron temperature in the *F2* region over the next 1.5 hours. The relevant radar observations (Figure 3 below) demonstrate that the equatorward and poleward boundaries of this particular ionospheric region are indeed found nearly at the same invariant latitudes as the boundaries of the intense soft-electron precipitation observed by DMSP-F7.

In Figure 3 we show the plasma density (a), the electron temperature (b), and the ion temperature (c), inferred from radar elevation scans, as stacks of clock dial plots in 50-km altitude steps. Time runs counterclockwise around the circle, with 14 UT (approximately 12 MLT) at the top; invariant latitude covers the range 68° to 80° from outward to inward. At each altitude, the DMSP-F7 pass is marked by a radial line with a heavy segment, which corresponds to the intense soft-electron precipitation region. The plasma density and temperature scaling bars change with altitude. The numbers printed to the right of the clock dials correspond to the fixed altitudes printed on the left. In each pair of scale numbers, the smaller number marks the upper limit of the blank bin; all densities or temperatures below this level and possible data gaps appear blank. The higher number marks the lower limit of the darkest shaded bin; all densities and temperatures exceeding this level fall into the darkest bin. Note that the data plotted in Figure 3—and also those plotted in Figure 4—do not represent a snapshot of the ionosphere, but rather a combination of spatial variation and temporal evolution sampled by the radar as it rotates, fixed to the earth, under the high-latitude ionosphere. Because of the interpolating software used to generate Figure 3, this figure might give the impression of a better resolution than is actually available: The antenna cycle time limited the temporal resolution (at a given latitude) to some 25 min. Specifically, the DMSP-F7 pass fell exactly between two elevation scans; thus, ionospheric plasma-density and temperature profiles are available only some 10 min before and after the pass.

At 150- and 200-km altitude, we notice scattered patches of enhanced electron density in the morning prior to the satellite pass and also in the afternoon. They are accompanied by elevated electron and ion temperatures. A careful examination shows that the elevated temperatures appear close to, but not spatially coincident with, the increased plasma density. A band of enhanced plasma density appears at 250- and 300-km altitude at the same invariant latitudes where DMSP-F7 observed intense soft-electron precipitation. This band begins with the DMSP-F7 pass and extends over about 1.5 hours. Because of the 20-min gap between two consecutive radar scans, it is more accurate to say that the radar did not observe enhanced plasma density in the scan before the pass, but observed it in the scan following the pass. (This applies also to the temperatures, discussed below.) The band of enhanced plasma density is about 2° wide in latitude. It is most pronounced at 250- and 300-km altitude and fades at higher altitudes. The enhanced plasma density coincides with elevated electron temperature. This is barely noticeable at 200-km altitude, but becomes more prominent with each upward altitude step. A slight ion temperature increase is seen only from 300 km upward and mainly at the poleward edge of the soft-electron flux region. At 400-km altitude, the ion temperature seems to coincide with the soft-electron precipitation, but unfortunately reasonably accurate radar data are scarce. At 350- and 400-km altitude, a plasma tongue in the equatorward part of the radar field of view between 1230 and 1430 UT gradually assumes dominance over the plasma density distribution.

However, it is not accompanied by increased electron and ion temperatures. This high-altitude plasma tongue is most likely the poleward tip of a region of enhanced dayside ionization generated by solar radiation that was subsequently advected into the polar cap. We do not show data from above 400 km because the radar return signals were weak and the temperatures were highly uncertain.

The radar data show that enhanced electron density, elevated electron temperature and slightly elevated ion temperature coincide only in a 2°-wide area along 74° invariant latitude, between 1230 and 1400 UT. This is most clearly seen in the data from 300 km altitude. This interval coincides with the latitude range where DMSP-F7 measured intense soft-electron precipitation, and we suggest that these particular ionospheric plasma properties are the result of intense soft (magnetosheath-like)-electron precipitation. Further down, we show that these signatures agree with predictions from an ionospheric model.

The radar observations of the plasma convection are plotted in Figure 4, also in a clock dial stack. The upper section shows results from the multiposition part of the antenna cycle, whereby it is assumed that drift magnitude and orientation with respect to the magnetic field are the same at both positions of a fixed position pair. The drift measured parallel to the geomagnetic field was used to construct the velocity vector. The lower section shows the drift inferred from the elevation scans using a method developed by *de la Beaujardière et al.* [1977]. In this method, *E*- and *F*-region line-of-sight ion velocities are merged, taking the different altitude dependencies of the Pedersen and Hall mobilities into account. Fixed-position radar measurements use only *F*-region data and cover a wider latitude range than the elevation scan measurements, which rely on *E*- and *F*-region data. The patterns obtained with the two different methods are very similar in the latitude range where they overlap, lending confidence to the convection pattern derived.

The hours around the DMSP-F7 pass are characterized by eastward (sunward) plasma drift reaching peak velocities of more than 2 km/s poleward of the radar while much smaller velocities are found equatorward of the radar. We notice a poleward turning of the plasma drift from 1230 UT onward in the equatorward section of the convection pattern, which we associate with the conjunction of the morning and afternoon convection cells. No IMF data are available for the time after 1030 UT; however, before 1030 UT, the B_y and B_z components of the IMF were negative (–9 nT and –4 nT, respectively) and remained relatively constant for many hours. We suspect that these IMF conditions prevailed after 1030 UT because the observed shift of the cusp toward prenoon is consistent with an IMF-$B_y < 0$ convection pattern [*Heelis*, 1984], and the intense soft-electron precipitation is consistent with magnetosheath plasma entry into the magnetosphere facilitated by a negative IMF-B_z component.

The radar ion flow measurements contain a gap (radar blind spot) in the vicinity of the radar location at 74° invariant and thus do not cover, on a small scale, the soft-electron flux region. Therefore we cannot deduce whether the convection reversal was within the cusp or at its equatorward or poleward boundary. In a steady-state situation, it is usually assumed that the cleft (which maps to the LLBL, cf. *Vasyliunas* [1979]) lies on closed and the cusp on open field lines, with the boundary between closed and open field lines coinciding with the convection reversal. *Foster et al.* [1989] indeed place the cusp/cleft boundary at the same latitude as the convection reversal. *Cowley et al.* [1991] argue that the boundary between open and closed field

lines lies poleward of the convection reversal, because of momentum transfer by viscous interaction at the magnetopause. It is also sometimes assumed that the cusp lies within the high-latitude convection throat, but *Lockwood* [1991] notes that, owing to the IMF-B_y dependence of the convection pattern, the throat is not a good indicator of the cusp position. We have examined several cases in which the location of the particle cusp was monitored by Sondrestrom radar measurements, and have found that in general neither the convection reversal nor the throat clearly determine the position of the cusp [*Watermann et al.*, 1993].

We now formulate our reasoning in a different way. Enhanced *F*-region electron concentration, if not locally produced, corresponds to a low electron-loss rate. This is a typical for small electric fields [e.g., *Schunk et al.*, 1975], unlike that measured within the poleward section of the soft-particle precipitation region. We also find an increase of the *F*-region electron energy loss rate within the particle cusp. We computed the rate of energy loss from electrons to ions and neutrals [*Kofman and Wickwar*, 1984] for different antenna positions of the multiposition part of that radar cycle that coincided with the DMSP-F7 pass. The total electron energy loss rate depends on neutral and charged particle density and neutral composition, as well as ion, electron, and neutral temperatures. Figure 5 shows this loss rate from observations in five radar positions close to the time of the DMSP pass. When the radar beam was parallel to the magnetic field (symbol F) and intersected the region of increased *F2* region electron density and temperature, the electron energy loss rate was significantly larger than on each of the two closest position pairs, one pair looking poleward (P) and the other equatorward (E). Because of the lower antenna elevation, the equatorward- and poleward-pointing radar beams remained within the field lines threaded by intense soft-electron precipitation only up to some 170-km altitude. The coincidence of high electron energy loss rates with high plasma density and elevated electron temperature in the *F* region strongly supports our view that this data set shows the effects of locally confined intense soft-particle precipitation into the ionosphere and subsequent electron energy loss to the ambient ion and neutral gas, as described by *Schunk and Nagy* [1978].

We have not reproduced diagrams from the other two days of the World Day campaign, 26 and 27 June. On 26 June the particle cusp was detected by DMSP-F7 poleward of the radar field of view and not at all on 27 June. Examination of the radar data from 26-27 June did not reveal signatures like those observed on 28 June, which we discussed above. Instead, on 26-27 June the daytime plasma density distribution showed a smooth slowly varying pattern, representative for a diurnal variation as expected from a stable sunlit ionosphere.

The magnetic perturbation along the DMSP-F7 trajectory was derived from DMSP-F7 magnetometer observations following the procedure of *Rich et al.* [1991]. Three-second averages of the horizontal perturbation vector (which is approximately perpendicular to the geomagnetic main field at this high latitude with 80° dip angle) are plotted in Figure 6. The magnetospheric regions associated with the observed particle fluxes are indicated, and the intense soft-electron precipitation interval is marked by a thick bar. In the CPS regime, a northwestward magnetic field perturbation prevails. Within the LLBL, its amplitude and orientation change considerably toward a larger and mainly west-southwest oriented magnetic perturbation field. From thereon throughout the cusp, the PM and the unidentified region the orientation changes very little. The amplitude, however, grows even larger within the PM to

reach its maximum near the poleward edge of the intense soft-electron flux interval, and then drops gradually to less than 100 nT in the polar rain region. Note that significant variations of either amplitude or orientation of the magnetic perturbation and its maximum amplitude occur within the different particle regions but not at their boundaries, with the only exception of the equatorward boundary of the polar rain. *De la Beaujardière et al.* [1993], who analyzed a larger set of DMSP passes through the dayside auroral zone, concluded that current intensifications (identified by sharp gradients in the magnetic field amplitude) and transitions between upward and downward currents (identified by the maximum amplitude of the magnetic perturbation) occur in general within the different particle regions and not at their boundaries. These particle and magnetic field measurements, made simultaneously on the same spacecraft, demonstrate that the distribution of field-aligned currents does in general not allow to determine the footprints of magnetospheric boundary regions and in particular the particle cusp.

We finish this section by summarizing the pertinent observational features from the 28 June 1984 event, which are sketched in Figure 7. Between 1230 and 1400 UT (approximately 10.5 to 12 MLT, i.e., close to magnetic noon) we observed a combination of spatially coincident and locally confined region characterized by enhanced *F2*-region plasma density, elevated electron temperature, slightly elevated ion temperature, and a high electron-energy-loss rate. The plasma temperature elevations dominate at the higher altitudes. The dark area shows the region where the Sondrestrom radar measured electron density and temperature in excess of 2×10^{11} m^{-3} and 2800 K, respectively, at 300-km altitude. The box on the DMSP-F7 trace indicates the interval where intense soft-electron precipitation was measured. The arrows delineate the plasma flow pattern. Because of the predominantly zonal plasma flow and the very small poleward flow components, it seems unlikely that the plasma patch constitutes remnant ionization from solar radiation that had drifted poleward into the radar field of view. If the patch were associated with the flow shear, it should appear as cool as the background plasma and also extend further along the flow reversal line into the afternoon sector. We suggest that the combined observations should be interpreted as an ionospheric signature of magnetosheath-like plasma precipitation.

MODEL PREDICTIONS

We have used an auroral model [*Lummerzheim*, 1987] to predict the ionospheric plasma density and temperature distribution relevant to this event. The model in its currently available one-dimensional version does not take into consideration horizontal diffusion and convection. It consists of two major parts, which are differentiated by the characteristic time scales of the included processes: The first part deals with transport of energetic particles and resulting excitation and ionization processes; the second part covers the thermospheric chemistry and diffusive transport. The major ionization sources used in this model include electron precipitation, solar EUV radiation, and photoelectrons.

Input parameters to the model are provided by specifying an electron flux spectrum above the ionosphere (but below the auroral acceleration zone), a thermosphere model (at present, the MSIS-90 model, see *Hedin* [1991]), and the day of the year and solar local time. The ionization rates obtained serve as input to the ion chemistry part, which is built on the reaction rates given

in the appendix of *Rees* [1989]. Finally, the electron and ion energy equations are solved. The model then predicts time-dependent vertical profiles of the plasma density, ion composition, and electron and ion temperatures, among other parameters.

This model allows for pitch-angle-dependent electron precipitation, but we cannot make use of this detail, because the DMSP spectrometers point always vertically upward and make only one-directional flux measurements. However, this does not pose a significant problem in the cusp because Viking measurements of pitch-angle-resolved cusp electron precipitation have shown that the cusp electron flux is virtually isotropic [*Aparicio et al.*, 1991]. Therefore, we feel it is justified to assume isotropy for the cusp electron spectra observed on DMSP-F7. Isotropy is not normally found in the LLBL precipitation [*Lundin*, 1988], therefore the DMSP particle measurements in the LLBL were not used for the model calculations.

For the model calculations, we reduced the atomic oxygen density obtained from the MSIS standard atmosphere by a factor of two, which led to a better agreement between radar observations and model predictions. Such a reduction factor is perhaps justified by reports that the MSIS model tends to overestimate the atomic oxygen abundance in the *E* region during times of auroral precipitation [*Hecht and Strickland*, 1988; *Lummerzheim et al.*, 1990]. As input spectrum to the model, we used an average over the spectra observed by DMSP-F7 in the interval labeled "cusp" in Figures 1, 2, and 6. Because DMSP-F7 measured the electron flux only above 30 eV energy we had to make assumptions about the extrapolation of the spectrum to lower energies. Test runs with different extrapolations showed that the modeled plasma density distribution does not change noticeably, but that the plasma temperatures above some 300 km altitude would change. The temperature distributions that we obtained are therefore only qualitatively valid above 300 km. In our simulation, we assumed that a corotating station entered a region of constant soft-electron precipitation at 0900 solar local time (SLT), equivalent to 1224 UT (i.e., the time of the DMSP-F7 pass over Sondrestrom), and left it at 1030 SLT (1354 UT).

Figure 8 shows in an altitude versus SLT frame the variations in ionospheric plasma density and temperatures predicted by the auroral model. The upper panel shows that the plasma density in the ionospheric *F* region increases continuously over the time of the precipitation activity. More detailed examination of the model output indicates that the peak plasma density approaches nearly saturation toward the end of the precipitation. The plasma-density enhancement is significant only above some 200-km altitude and reaches a peak density of about 2.5 times the quiet preprecipitation state. The electron temperature reacts immediately to the precipitation onset; the temperature (and consequently the scale height) rise sharply and continue to rise as long as the precipitation is sustained. This temperature effect is seen only at higher altitudes, above some 180 km, and becomes more pronounced with increasing altitude. Two and a half hours after the precipitation finishes, the electron density and temperature resume their normal (solar-radiation-controlled) level. The ion temperature reacts slower, the temperature increase is marginal below 400 km and significant only at higher altitudes.

The characteristic features of the model simulation include a gradual increase of the *F*-region plasma density to a peak in the 200- to 300-km altitude range, an immediate increase of

the electron temperature at all *F*-region altitudes, but most pronounced at altitudes higher than the *F*-region density peak, and a slight increase of the ion temperature which is delayed in time and becomes significant only at the highest altitudes.

For comparison, we have run the model with an input electron spectrum as measured by DMSP-F7 around 1222:50 UT, i.e., at the time of the most intense CPS precipitation (see Figure 1). The model output shows detectable enhancements in the plasma density only below some 130 km but not in the *F* region, very small elevation in electron temperature from some 150 km upward, and no change in the ion temperature. The plasma density and temperature predictions shown in Figure 8 are thus clearly indicative of soft-electron precipitation.

DISCUSSION AND CONCLUSIONS

We have demonstrated that the ionospheric footprint of soft-electron precipitation can be identified from ground-based incoherent-scatter radar observations. In the event discussed here, the DMSP-F7 spacecraft traversed a region of intense soft (magnetosheath-like) electron flux, which included the LLBL, the cusp, and the equatorward section of the PM. The distinction between these regions from DMSP observations of particle characteristics is based mainly on the properties of the ion flux. This is consistent with *Johnstone* [1985], who claims that cusp and PM electrons are magnetosheath-like and therefore indistinguishable while the respective proton energy distributions differ. Because the intensity of the ion-energy flux is an order of magnitude or more below that of the electron flux, we do not expect that we can distinguish these three regions by their ionospheric signatures. Radar observations of plasma density and temperature show indeed a correlation with the intense soft-particle flux region, but the radar measurements do not allow to resolve a further subdivision, because of the similar electron spectra in these three regions and the limited resolution of the radar data.

The agreement between model results and radar observations of *F*-region plasma density and temperature distributions, although not fully satisfactorily, lends confidence to the ionospheric model and to our interpretation of our radar observations. The largest discrepancy appears in the plasma density distribution: The *F*-region peak density measured with the radar reaches only about 3×10^{11} m^{-3} within the precipitation region, and the model predicts almost 8×10^{11} m^{-3}. The agreement between the measured and modeled electron temperatures is much better: radar data from 300 km altitude, just above the *F*-region density peak, show an electron temperature maximum of some 3000 K, while the model gives at this altitude 2900 K soon after the precipitation onset and 2300 K after the precipitation has lasted for at least one hour. Model calculations and radar observations of ion temperatures near the *F*-region peak show very little dependence on presence or absence of precipitation. It is interesting to note that the differences between measurements and model predictions are systematic. Before, during, and after the precipitation, the modeled plasma density is higher than the measured, and the modeled electron and ion temperatures are lower than the measured.

We may speculate about the reason for the discrepancy between observations and model predictions by comparing measurements from 28 June to those of 27 June. On 27 June, DMSP-F7 measured electron precipitation of about 1 keV average energy and 0.8×10^{-3} J m^{-2} s^{-1} average integrated energy flux between 72° and 76° invariant latitude. On 28 June, the

corresponding numbers valid for the cusp interval are 100-150 eV average energy and 1.6×10^{-3} J m^{-2} s^{-1} energy flux. On 27 June, electron precipitation had therefore much less effect on the ionospheric *F* region above the radar than on 28 June. However, on 27 June, the *F*-region peak density measured on the field line through the radar site hovered around 2.5×10^{11} m^{-3} during several hours from late morning into the afternoon, compared to 1.7×10^{11} m^{-3} (outside the cusp region) on 28 June. On 27 June, the *Kp* index did not exceed 20 and the *AE* value stayed below 200 nT during the daytime hours while on June 28 the *Kp* index reached 40 and *AE* some 1000 nT, i.e., there was significantly higher geomagnetic and electrojet activity, consistent with the observed large plasma velocities on 28 June (see Figure 4) which exceeded 1000 m/s in the poleward part of the radar field of view. According to *Schunk et al.* [1975], Eqs. (16)-(22), a 1000-m/s plasma drift (or, equivalently, a 50-mV/m electric field) would increase the effective *F*-region ion temperature by about 800 K over the neutral temperature. Such a temperature increase results in higher O^+ reaction rates and consequently reduced plasma density because the molecular ions recombine much faster than atomic oxygen. Our auroral model, which is one-dimensional, cannot account for the effects of the large electric field. The high geomagnetic and electrojet activity on 28 June therefore provides a possible explanation for the observed discrepancy between measurements and model predictions.

This event and a few others that we examined demonstrate that an incoherent-scatter radar can identify regions of soft-particle precipitation by their *F* region signatures. We assume that these regions are threaded by open field lines connected to the exterior cusp and to magnetospheric boundary layers such as the LLBL (at least sometimes) and the PM. The open field lines allow the magnetosheath plasma a more or less direct access to ionospheric altitudes. Whether it will in general be possible to distinguish the footprint of the particle cusp from the LLBL and PM with ground-based observations is still an open question. One of the principal difficulties concerns the ion precipitation. *Hardy et al.* [1989] have shown that the ion energy flux along the noon-midnight meridian is on the average an order of magnitude below the electron energy flux at all levels of geomagnetic activity. While spaceborne particle spectrometers can determine the characteristics of the ion precipitation irrespective of electron precipitation, the ionospheric response (ionization and plasma thermalization) is dominated by the more intense electron precipitation. In this particular event, we also faced the problem of the limited spatial resolution of the radar measurements. From an analysis of Viking data, *Aparicio et al.* [1991] found the average width of the statistical cusp (including cusp proper, boundary cusp and mantle cusp) to be 2° in magnetic latitude, while *Newell and Meng* [1988, 1992] determined from DMSP-F7 and -F9 observations an average (but highly variable) cusp width of about 1°. In future experiments, we will therefore operate the Sondrestrom radar in a mode that provides better spatial resolution than was achieved in previously performed experiments.

It remains the question how the ionospheric electrostatic potential distribution (or equivalently the plasma convection pattern) is related to the particle cusp. The example discussed here as well as some other cases that we have examined indicate that measurements of the *F*-region plasma density and temperature distributions have the potential of being a much better cusp identifier than the distribution of the plasma convection. We also emphasize that the magnetic perturbation field measured by DMSP-F7 does not exhibit significant changes in

amplitude or orientation that coincide with the equatorward and poleward boundaries of the particle cusp. Because the magnetic perturbation conveys information about the field-aligned currents, we find that field-aligned currents cannot serve as a cusp identifier either.

We acknowledge that analysis of a few individual events is not sufficient to determine how and under which conditions the particle cusp or more generally a flux tube filled with magnetosheath plasma can reliably be identified from incoherent scatter radar measurements. We plan to examine more coincident radar and spacecraft data to determine if particular geophysical conditions facilitate observation of such signatures with the radar.

Acknowledgment. This work was supported by the National Science Foundation through the Cooperative Agreement ATM-8822560 with SRI International and through Grants ATM-9112680 to SRI, ATM-9022197 to UAF, and ATM-9108193 to APL/JHU. NASA support was provided under Contract NASW-4603 with SRI and Grant NAGW-3037 to UAF.

REFERENCES

Aparicio, B., B. Thelin, and R. Lundin, The polar cusp from a particle point of view: A statistical study based on Viking data, *J. Geophys. Res., 96*, 14023, 1991.

Baker, K.B., R.A. Greenwald, J.M. Ruohoniemi, J.R. Dudeney, M. Pinnock, P.T. Newell, M.E. Greenspan, and C.-I. Meng, Simultaneous HF-radar and DMSP observations of the cusp, *Geophys. Res. Lett., 17*, 1869, 1990.

Bythrow, P.F., T.A. Potemra, R.E. Erlandson, L.J. Zanetti, and D.M. Klumpar, Birkeland currents and charged particles in the high-latitude prenoon region: A new interpretation, *J. Geophys. Res., 93*, 9791, 1988.

Cowley, S.W.H., J.P. Morelli, and M. Lockwood, Dependence of convective flows and particle precipitation in the high-latitude dayside ionosphere on the *X* and *Y* components of the interplanetary magnetic field, *J. Geophys. Res., 96*, 5557, 1991.

de la Beaujardière, O., J. Watermann, P. Newell, and F. Rich, Relationship between Birkeland current regions, particle precipitation, and electric fields, *J. Geophys. Res.*, 1993.

de la Beaujardière, O., R. Vondrak, and M. Baron, Radar observations of electric fields and currents associated with auroral arcs, *J. Geophys. Res., 82*, 5051, 1977.

Engebretson, M.J., B.J. Anderson, L.J. Cahill, Jr., R.L. Arnoldy, T.J. Rosenberg, D.L. Carpenter, W.B. Gail, and R.H. Eather, Ionospheric signatures of cusp latitude Pc 3 pulsations, *J. Geophys. Res., 95*, 2447, 1990.

Engebretson, M.J., C.-I. Meng, R.L. Arnoldy, and L.J. Cahill, Jr., Pc 3 pulsations observed near the polar cusp, *J. Geophys. Res., 91*, 8909, 1986.

Foster, J.C., H.-C. Yeh, J.M. Holt, and D.S. Evans, Two-dimensional mapping of dayside convection, in *Electromagnetic Coupling in the Polar Clefts and Caps*, edited by P. E. Sandholt and A. Egeland, pp 115-125, Kluwer, Dordrecht/Boston/London, 1989.

Hardy, D.A., L.K. Schmitt, M.S. Gussenhoven, F.J. Marshall, H.C. Yeh, T.L. Shumaker, A. Hube, and J. Pantazis, Precipitating electron and ion detectors (SSJ/4) for the block 5D/flights 6-10 DMSP satellites: Calibration and data presentation, *Rep. AFGL-TR-84-0317*, Air Force Geophys. Lab., Hanscom Air Force Base, Mass., 1984.

Hardy, D.A., M.S. Gussenhoven, and D. Brautigam, A statistical model of auroral ion precipitation, *J. Geophys. Res., 94*, 370, 1989.

Haerendel, G., G. Paschmann, N. Sckopke, H. Rosenbauer, and P.C. Hedgecock, The Frontside boundary layer of the magnetosphere and the problem of reconnection, *J. Geophys. Res., 83*, 3195, 1978.

Hecht, J.H., and D.J. Strickland, Measurements of *E* region atomic oxygen densities deduced from permitted optical auroral emissions and from incoherent scatter radar data (abstract), *Eos Trans. AGU, 69*, 1346, 1988.

Hedin, A.E., Extension of the MSIS thermosphere model into the middle and lower atmosphere, *J. Geophys. Res., 96*, 1159, 1991.

Heelis, R.A., The effects of interplanetary magnetic field orientation on dayside high-latitude ionospheric convection, *J. Geophys Res.*, 2873, 1984.

Johnstone, A.D., Electron injection in the polar cusp, in *The Polar Cusp*, edited by Jan A. Holtet and Alv Egeland, pp. 47-63, Reidel, Dordrecht/Boston/Lancaster, 1985.

Kelly, J.D., Sondrestrom radar — initial results, *Geophys. Res. Lett., 10*, 1112, 1983.

Kofman, V., and V.B. Wickwar, Very high electron temperatures in the daytime F region at Sondrestrom, *Geophys. Res. Lett., 11*, 919, 1984.

Kremser, G., and R. Lundin, Average spatial distributions of energetic particles in the midaltitude cusp/cleft region observed by Viking, *J. Geophys. Res., 95*, 5753, 1990.

Lockwood, M., Incoherent scatter radar measurements of the cusp, ESA-SP, 1991.

Lummerzheim, D., Electron transport and optical emissions in the aurora, Ph.D. thesis, University of Alaska, Fairbanks, 1987.

Lummerzheim, D., M.H. Res, and G.J. Romick, The application of spectroscopic studies of the aurora to thermospheric neutral composition, *Planet. Space Sci., 38*, 67, 1990.

Lundin, R., Acceleration/heating of plasma on auroral field lines: Preliminary results from the Viking satellite, *Ann. Geophys., 6*, 143, 1988.

Lundin, R., Magnetopause boundary layers, *J. Geomag. Geoelectr., 43*, Suppl., 165, 1991.

McEwen, D.J., Optical-particle characteristics of the polar cusp, in *The Polar Cusp*, edited by Jan A. Holtet and Alv Egeland, pp. 193-202, Reidel, Dordrecht/Boston/Lancaster, 1985.

McHarg, M.G., and J.V. Olson, Correlated optical and ULF magnetic observations of the winter cusp-boundary layer system, *Geophys. Res. Lett., 19*, 817, 1992.

Newell, P.T., and C.-I. Meng, On quantifying the distinctions between the cusp and the cleft/LLBL, in *Electromagnetic Coupling in the Polar Clefts and Caps*, edited by P. E. Sandholt and A. Egeland, pp 87-101, Kluwer, Dordrecht/Boston/London, 1989.

Newell, P.T., and C.-I. Meng, The cusp and the cleft/boundary layer: Low-altitude identification and statistical local time variation, *J. Geophys. Res., 93*, 14549, 1988.

Newell. P.T., and C.-I. Meng, Mapping the dayside ionosphere to the magnetosphere according to particle precipitation characteristics, *Geophys. Res. Lett., 19*, 609, 1992.

Olson, J.V., ULF signatures of the polar cusp, *J. Geophys. Res., 91*, 10055, 1986.

Rees, M.H., *Physics and Chemistry of the Upper Atmosphere*, Cambridge Atmospheric and Space Science Series, Cambridge University Press, 1989.

Rich, F.J., M.S. Gussenhoven. D.A. Hardy, and E. Holeman, Average height-integrated Joule heating rates and magnetic deflection vectors due to field-aligned currents during sunspot minimum, *J. Atmos. Terr. Phys., 53*, 293, 1991.

Sandholt, P.E., A. Egeland, J.A. Holtet, B. Lybekk, K. Svenes, and S. Åsheim, Large- and small-scale dynamics of the polar cusp region, in *The Polar Cusp*, edited by Jan A. Holtet and Alv Egeland, pp. 163-175, Reidel, Dordrecht/Boston/Lancaster, 1985.

Schunk, R.W., and A.F. Nagy, Electron temperatures in the F region of the ionosphere: Theory and observations, *Rev. Geophys. Space Phys., 16*, 355, 1978.

Schunk, R.W., W.J. Raitt, and P.M. Banks, Effect of electric fields on the daytime high-latitude *E* and *F* regions, *J. Geophys. Res., 80*, 3121, 1975.

Sivjee, G.G., The effects of magnetosheath electrons on charge exchange, radiation trapping and other atomic and molecular processes in the mid-day polar cusp thermosphere, in *The Polar Cusp*, edited by Jan A. Holtet and Alv Egeland, pp. 111-126, Reidel, Dordrecht/Boston/Lancaster, 1985.

Vasyliunas, V.M., Interaction between the magnetospheric boundary layers and the ionosphere, *Magnetospheric Boundary Layers*, edited by B. Battrick, ESA SP-148, 87, 1979.

Watermann, J., O. de la Beaujardière, and P.T. Newell, Incoherent scatter radar observations of ionospheric signatures of cusp-like electron precipitation, *J. Geomag. Geoelec.*, 1993.

Wickwar, V.B., and W. Kofman, Dayside red auroras at very high latitudes: The importance of thermal excitation, *Geophys. Res. Lett, 11*, 923, 1984.

FIGURE CAPTIONS

Fig. 1. DMSP-F7 measurements of particle precipitation during a cusp pass over Sondrestrom on 28 June 1984 around 1224 UT. Top panel: electron and ion band integrated energy flux and average energy; middle and bottom panels: electron and ion energy flux spectrograms (30 eV to 30 keV) in eV cm^{-2} s^{-1} sr^{-1} eV^{-1}, with the ion ordinate reversed.

Fig. 2. The DMSP-F7 pass of 28 June 1984, mapped down to 120-km altitude and projected on a geographic grid with dotted contours of equal invariant latitude. Also shown are the Sondrestrom radar location (diamond labeled SSF) with the antenna elevation scan trace at 120 km (thick) and 350 km (thin) and the location of the particle cusp during the previous DMSP pass. The regions with intense soft-electron precipitation and increased *F2*-region electron density and temperature are indicated by hatched segments.

Fig. 3. Plasma density (a), electron temperature (b) and ion temperature (c) in clock dial stacks with 50-km altitude separation. Time runs counterclockwise, invariant latitude covers the range from 69° to 80° from outside to inside. Note that the gray scale varies with altitude, as indicated by the pair of numbers written on the same line as the altitude. The heavy segment on the DMSP-F7 trajectory (between 12 and 13 UT) marks the region of intense soft-electron flux.

Fig. 4. Plasma flow pattern inferred from multiple fixed antenna positions (top) and elevation scans (bottom) of the Sondrestrom radar. Clock dial representation with DMSP pass as in Fig. 3.

Fig. 5. Electron energy loss rates (in eV cm^{-3}) from radar measurements at three fixed antenna positions around the time of the DMSP-F7 pass. P = incidates antenna pointing poleward, F = field-aligned, E = equatorward. In the field-aligned position, the radar beam intersects the high-density, high-temperature *F*-region plasma and shows the highest energy-loss rate.

Fig. 6. Horizontal magnetic deflection vector measured by DMSP-F7 along its trajectory as shown in Fig. 1. The different magnetospheric regions are indicated, the interval of intense soft-electron flux (covering LLBL, cusp, and the equatorward part of the PM) is marked by a thick line.

Fig. 7. Schematic diagram of incoherent-scatter radar observations during the DMSP-F7 cusp pass on 28 June 1984.

Fig. 8. Model calculations of plasma density and electron and ion temperature distributions over time under the influence of solar radiation and soft-particle precipitation (effective between 9 and 10.5 local time) as measured on board DMSP-F7. The model is one-dimensional, i.e., no plasma convection is included.

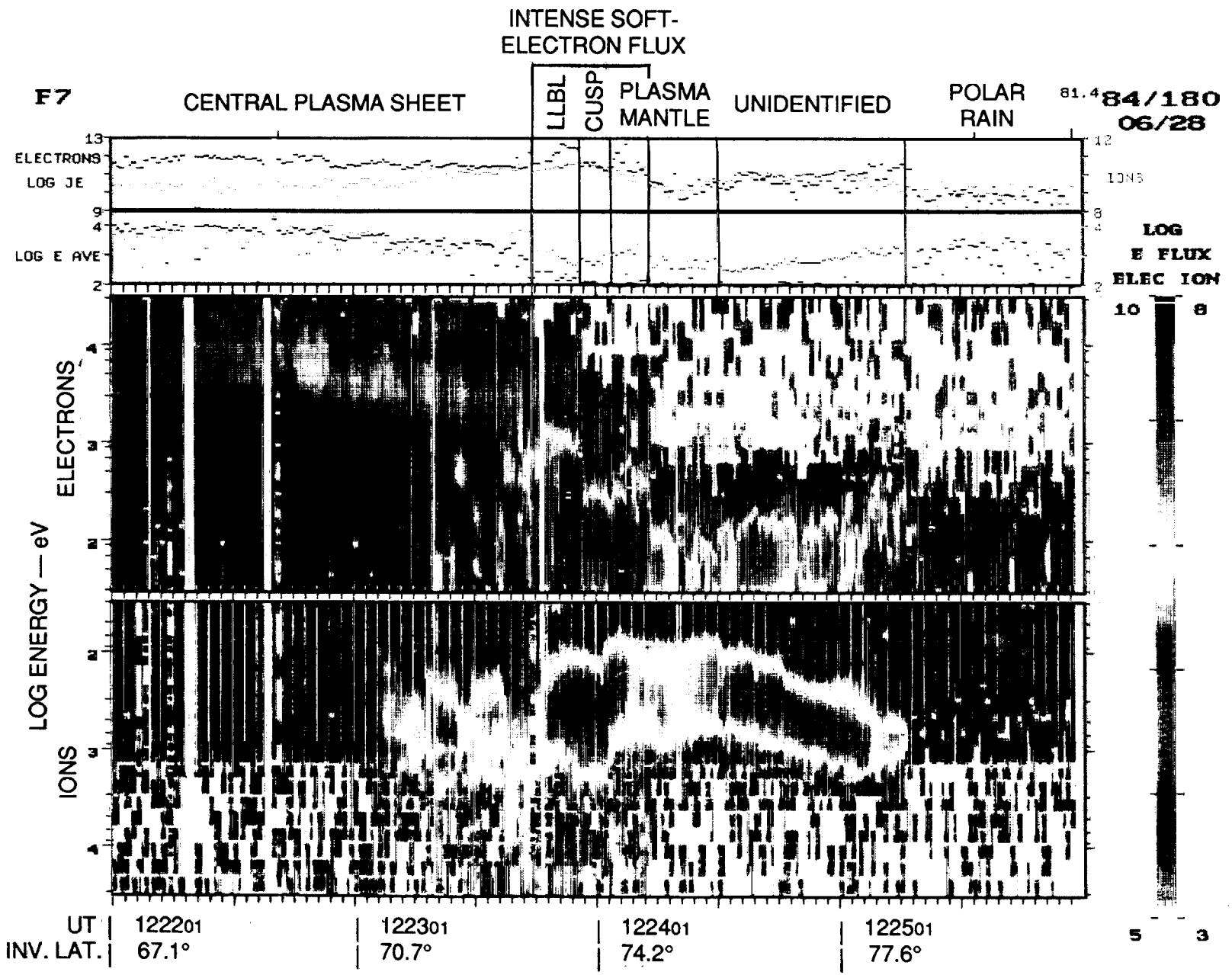
INTENSE SOFT-
ELECTRON FLUX
F7
CENTRAL PLASMA SHEET
LLBL
CUSP
PLASMA
MANTLE
UNIDENTIFIED
POLAR
RAIN
81.4 84/180
06/28
ELECTRONS
LOG JE
LOG E AVE
IONS
LOG
E FLUX
ELEC ION
LOG ENERGY — eV
ELECTRONS
IONS
UT
INV. LAT.
122201
67.1°
123301
70.7°
124401
74.2°
125501
77.6°

Fig. 1

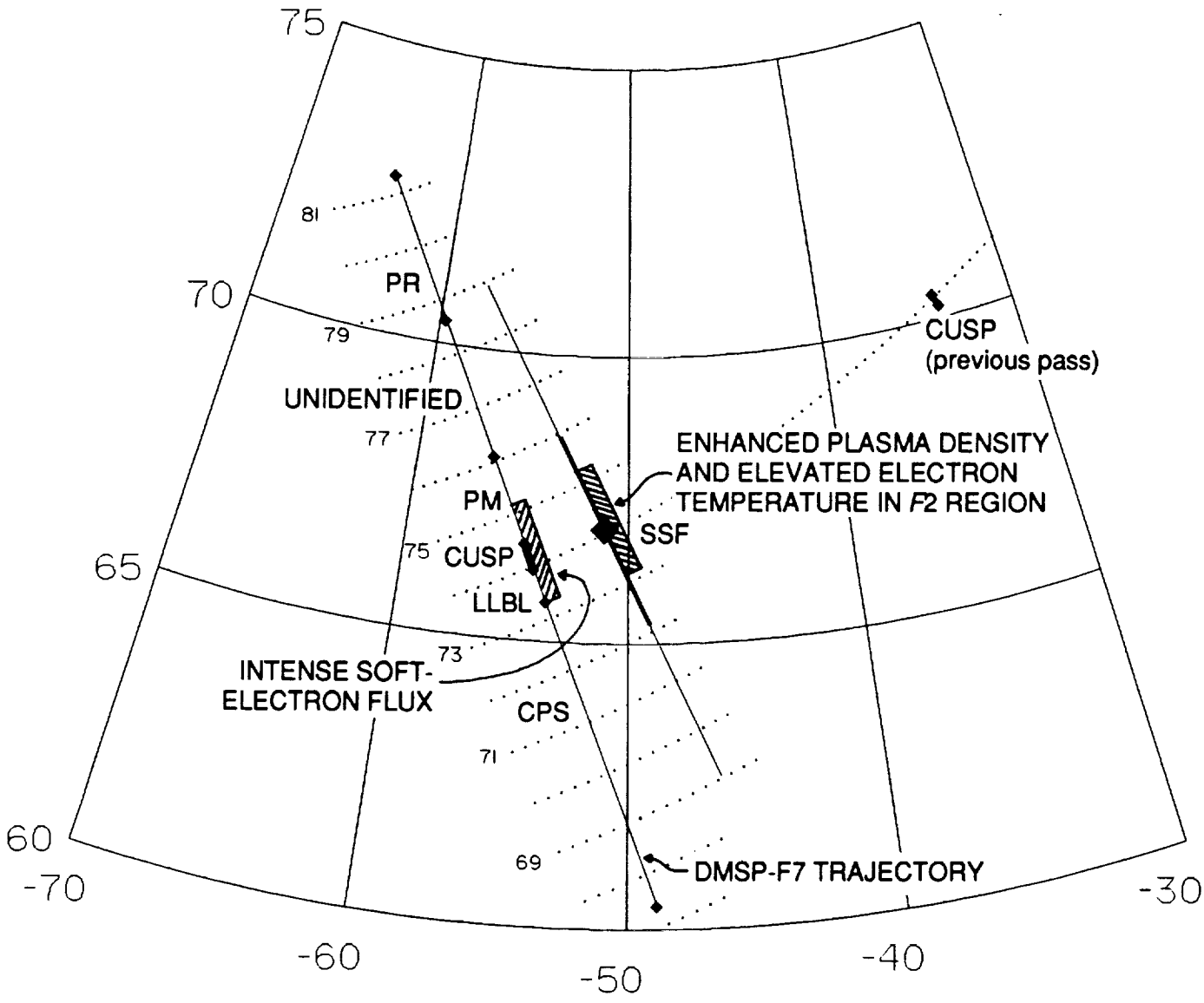
75
70
65
60
-70
-60
-50
-40
-30
81
79
77
75
73
71
69
PR
UNIDENTIFIED
PM
CUSP
LLBL
INTENSE SOFT-
ELECTRON FLUX
CPS
SSF
CUSP
(previous pass)
ENHANCED PLASMA DENSITY
AND ELEVATED ELECTRON
TEMPERATURE IN F2 REGION
DMSP-F7 TRAJECTORY

Fig. 2

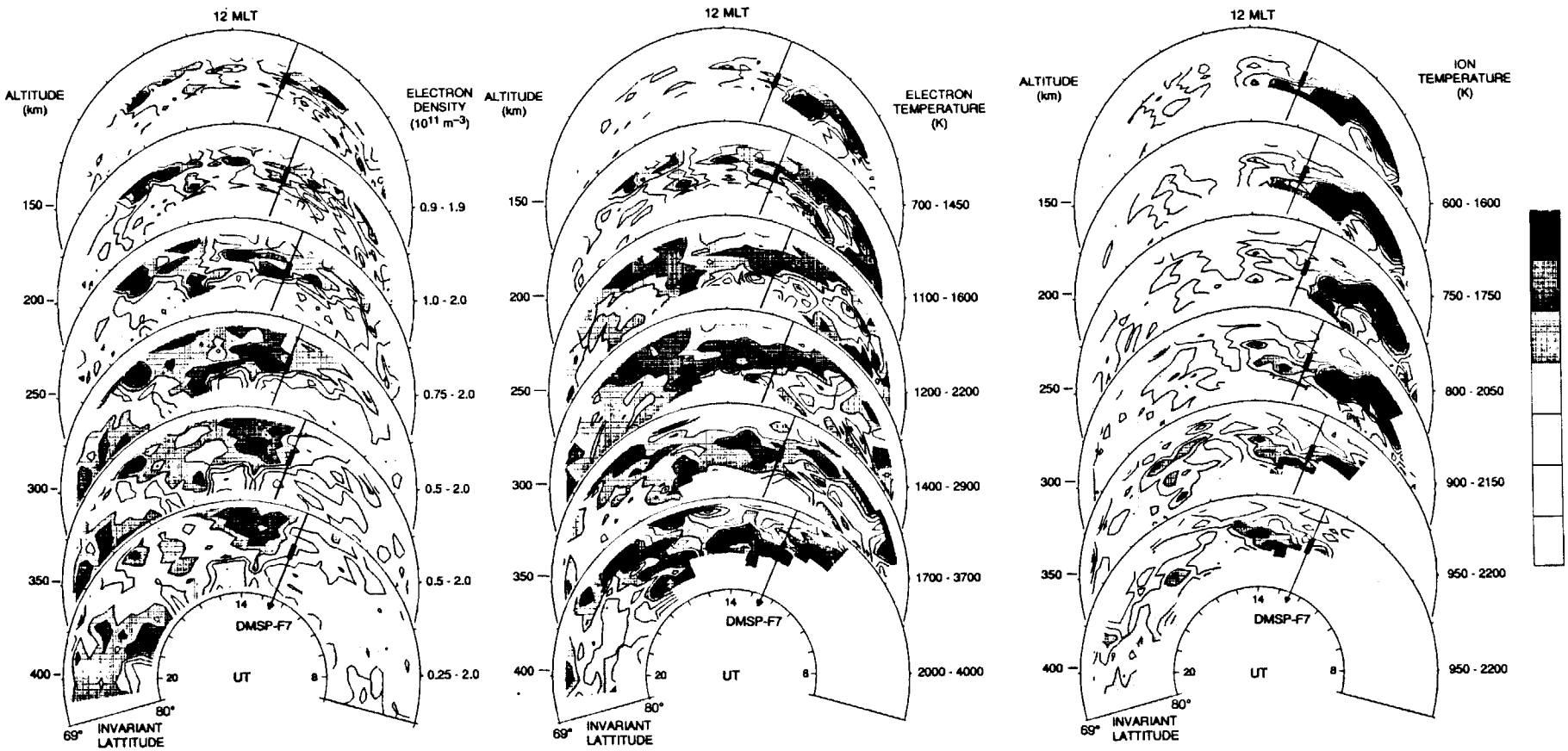
12 MLT
ALTITUDE (km)
ELECTRON DENSITY (10^{11} m^{-3})
150
200
250
300
350
400
0.9 - 1.9
1.0 - 2.0
0.75 - 2.0
0.5 - 2.0
0.5 - 2.0
0.25 - 2.0
14
DMSP-F7
20
UT
8
80°
69°
INVARIANT LATTITUDE
(a)
12 MLT
ALTITUDE (km)
ELECTRON TEMPERATURE (K)
700 - 1450
1100 - 1600
1200 - 2200
1400 - 2900
1700 - 3700
2000 - 4000
DMSP-F7
UT
INVARIANT LATTITUDE
(b)
12 MLT
ALTITUDE (km)
ION TEMPERATURE (K)
600 - 1600
750 - 1750
800 - 2050
900 - 2150
950 - 2200
950 - 2200
DMSP-F7
UT
INVARIANT LATTITUDE
(c)

Fig. 3

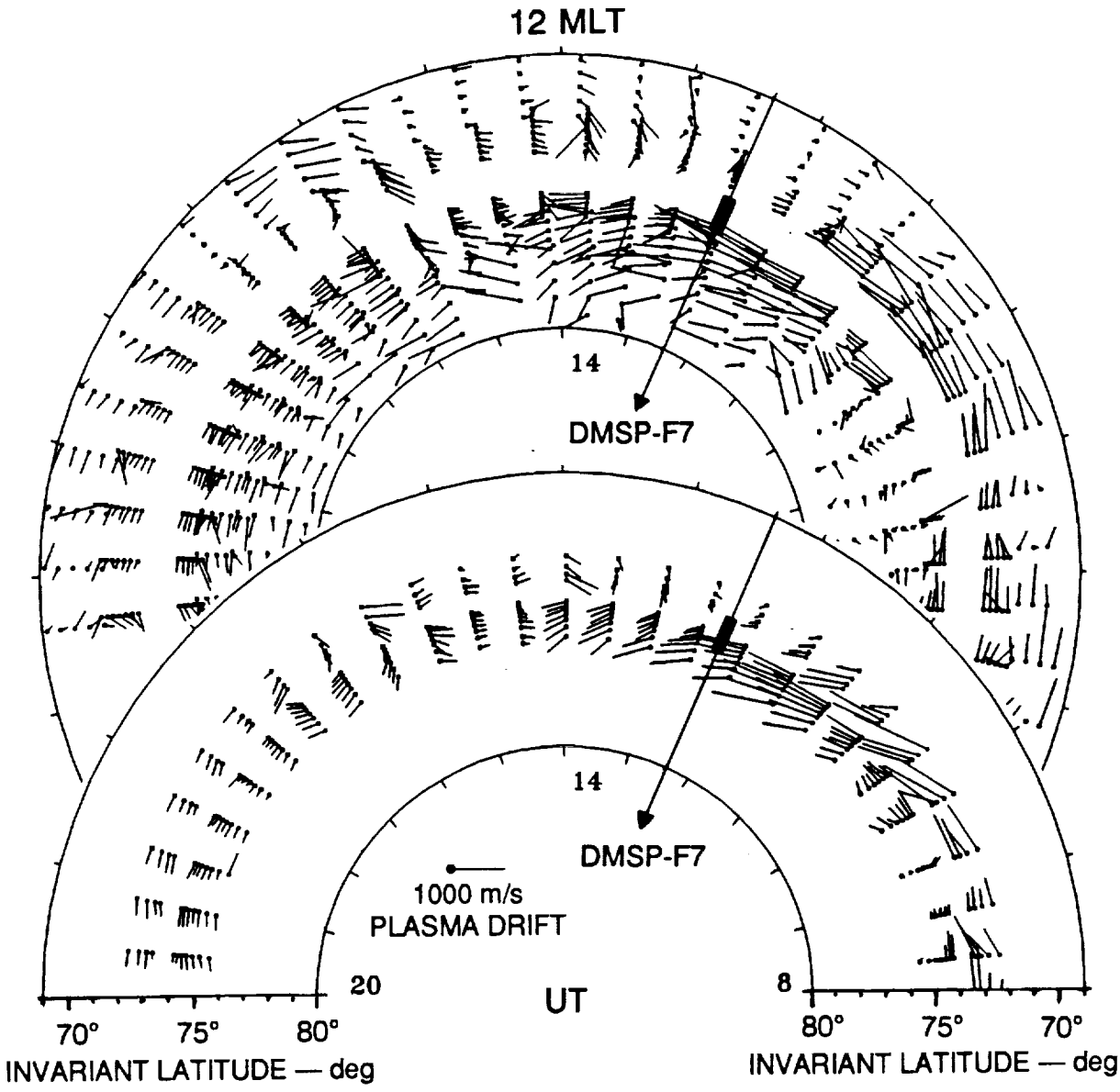
12 MLT
14
DMSP-F7
14
DMSP-F7
1000 m/s
PLASMA DRIFT
20
UT
8
70°
75°
80°
INVARIANT LATITUDE — deg
80°
75°
70°
INVARIANT LATITUDE — deg

Fig. 4

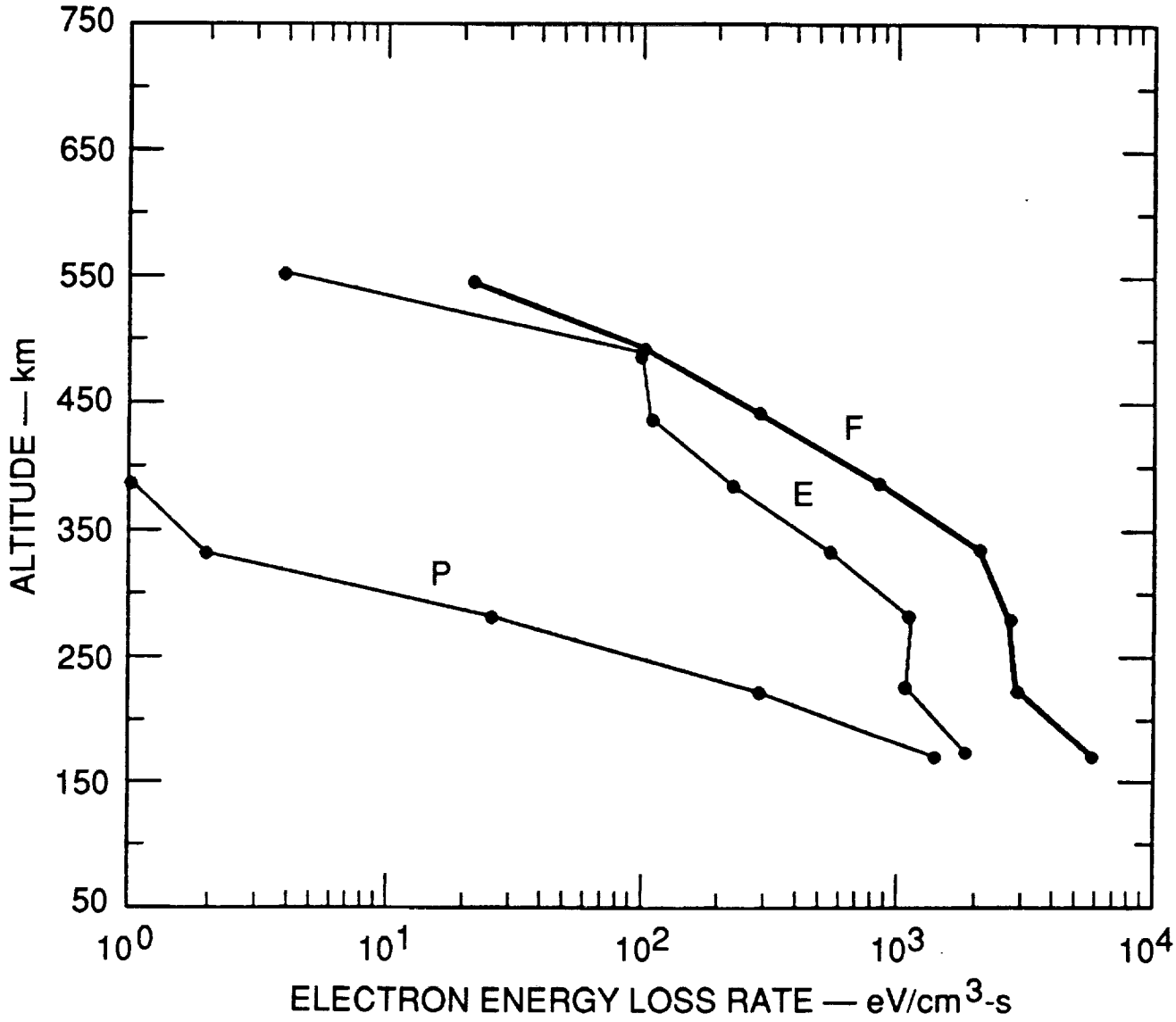
750
650
550
450
350
250
150
50
ALTITUDE — km
F
E
P
10^0
10^1
10^2
10^3
10^4
ELECTRON ENERGY LOSS RATE — eV/cm^3-s

Fig. 5

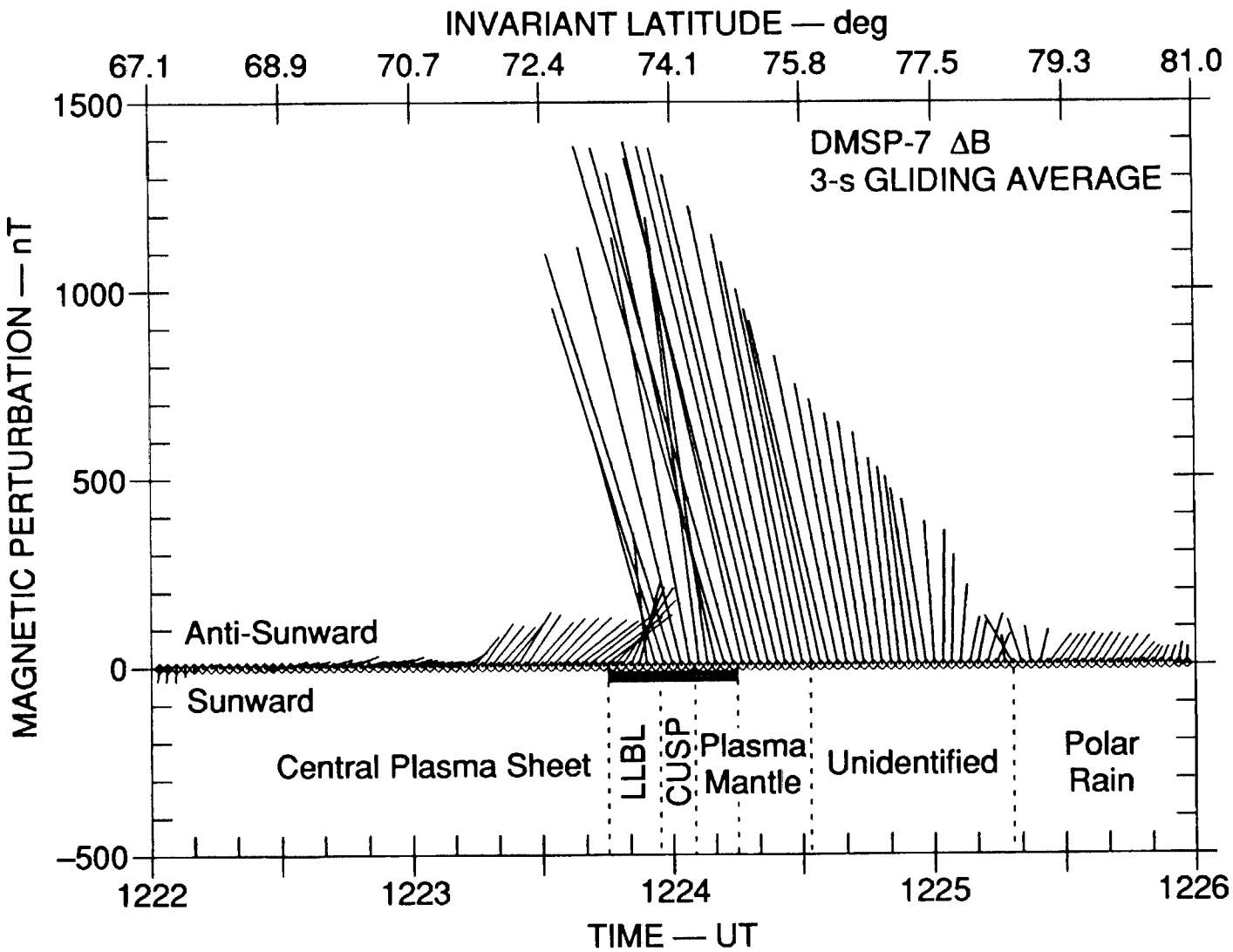
INVARIANT LATITUDE — deg
67.1
68.9
70.7
72.4
74.1
75.8
77.5
79.3
81.0
1500
1000
500
0
−500
MAGNETIC PERTURBATION — nT
DMSP-7 ΔB
3-s GLIDING AVERAGE
Anti-Sunward
Sunward
Central Plasma Sheet
LLBL
CUSP
Plasma Mantle
Unidentified
Polar Rain
1222
1223
1224
1225
1226
TIME — UT

Fig. 6

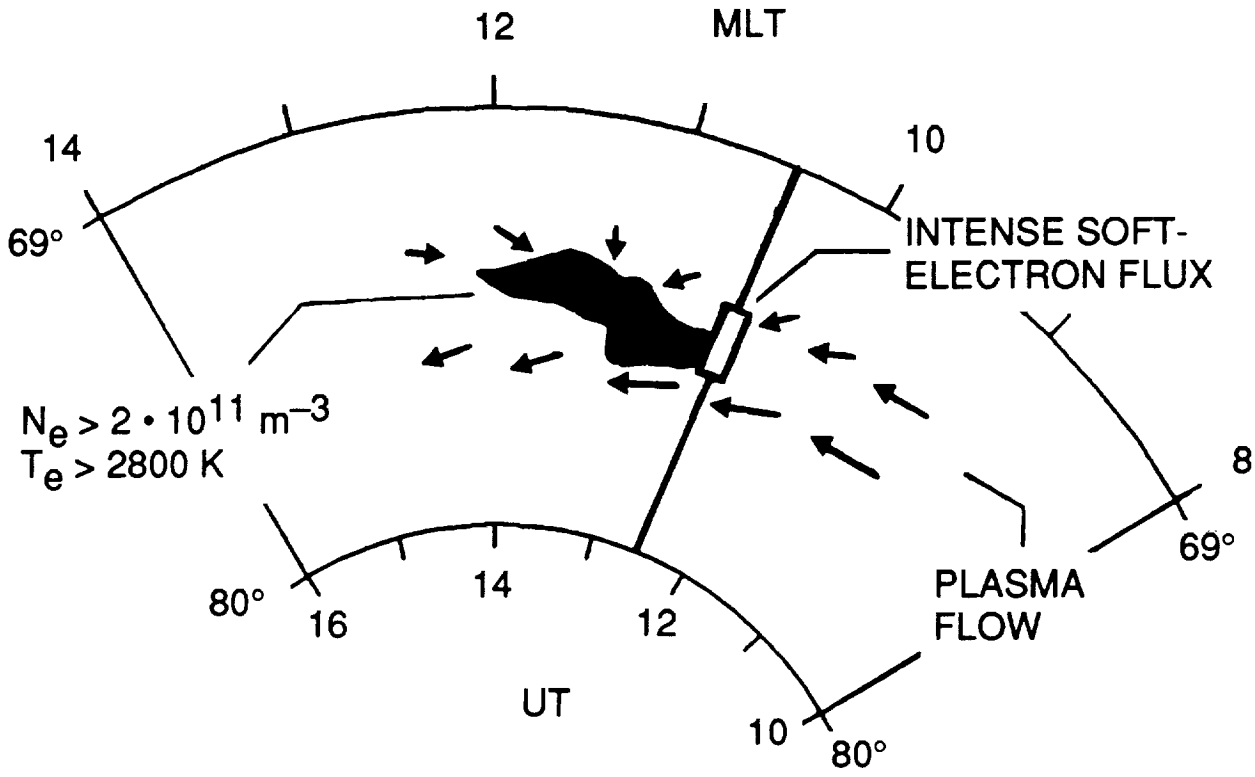
12
MLT
14
10
69°
INTENSE SOFT-
ELECTRON FLUX
$N_e > 2 \cdot 10^{11}$ m^{-3}
$T_e > 2800$ K
8
69°
80°
16
14
12
PLASMA
FLOW
UT
10
80°

Fig. 7

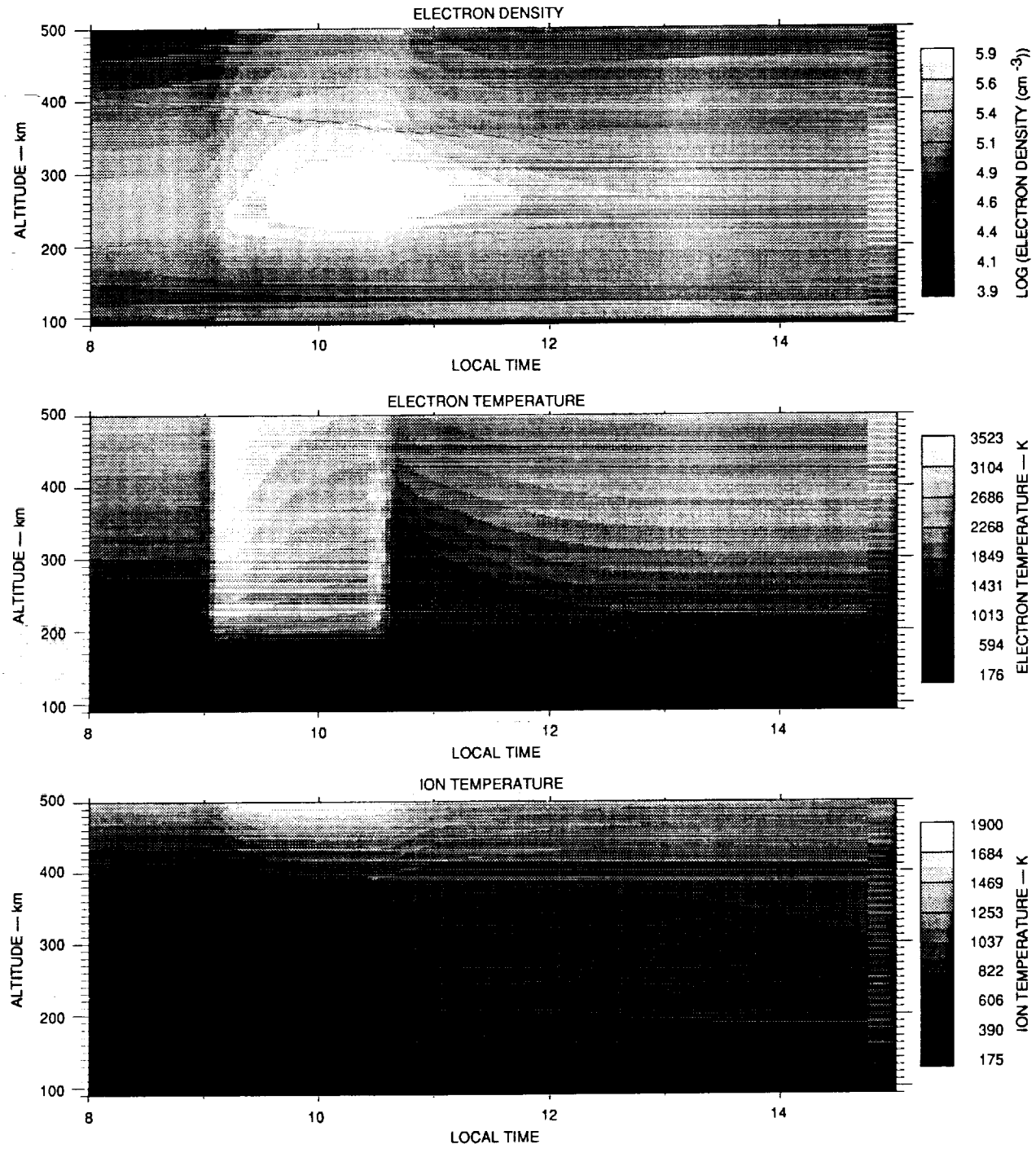
ELECTRON DENSITY
ALTITUDE — km
500
400
300
200
100
8
10
12
14
LOCAL TIME
5.9
5.6
5.4
5.1
4.9
4.6
4.4
4.1
3.9
LOG (ELECTRON DENSITY (cm -3))
ELECTRON TEMPERATURE
ALTITUDE — km
LOCAL TIME
3523
3104
2686
2268
1849
1431
1013
594
176
ELECTRON TEMPERATURE — K
ION TEMPERATURE
ALTITUDE — km
LOCAL TIME
1900
1684
1469
1253
1037
822
606
390
175
ION TEMPERATURE — K

Fig. 8